Joint SIP and TEM Measurements on an active Fumarole Field - Results from the 5th Vulcano Summer School 2019

Jana H. Börner[1], Mathias Scheunert[1], Franziska Mai[2], Carolin Schneider[1], and Klaus Spitzer[1]

[1] *Technical University Bergakademie Freiberg, Institute of Geophysics and Geoinformatics, Freiberg, Germany*
[2] *Technical University Berlin, Department of Applied Geophysics, Berlin, Germany*

Abstract

In the context of an interdisciplinary science convention, the Europlanet Vulcano Summer School 2019, joint SIP and TEM measurements were realized on an active fumarole field within a fault zone in the northern part of the island Vulcano (Italy). The aim of the field survey was to investigate the applicability of the two methods for imaging subsurface features such as gas migration paths and alteration products. The present work examines characteristics of fumaroles and draws a first positive balance from the preliminary evaluation of the observed EM data.

1 Introduction

The Vulcano Summer School is an interdisciplinary science congress that has now been organized for the fifth time by Jacobs University (Bremen) and DLR (Berlin). It aims at bringing together scientists from geology, astrobiology, oceanography, volcanology, geophysics and robotics as well as students and technicians from all over the world. The main concern is to test measuring equipment and robots under extreme conditions (high temperatures, dry ash and acidifying gases) in order to simulate interplanetary research cruises. Therefore, Vulcano acts as a Moon / Mars analogue site due to its volcanic activity including dry and rocky plateaus, fumaroles ejecting sulphuric gases among others and an allover dry and hostile environment. Besides that, the Vulcano Summer School enables students to undertake interdisciplinary training with a special focus on practical application. Due to its scientific value, funding is provided by the Europlanet program of the European Union (Unnithan et al., 2019).
The island of Vulcano (Fig. 1) is the third largest island of the Aeolian archipelago, situated approximately 20 km north of Sicily, Italy. Its seamount morphology built up in the last 150 000 years, but geologic formations get younger moving north and north-west (De Astis et al., 2013). The volcanism that is active up to the present time is driven by the subduction process of the African plate which is converging with the Apulian plate. This process becomes visible also in the known volcanoes Etna and Mount Vesuvius. The shape of Vulcano is dominated by the cone La Fossa di Vulcano, an active volcano that is located within two intersecting multi-stage calderas. Its last eruption took place in 1890.

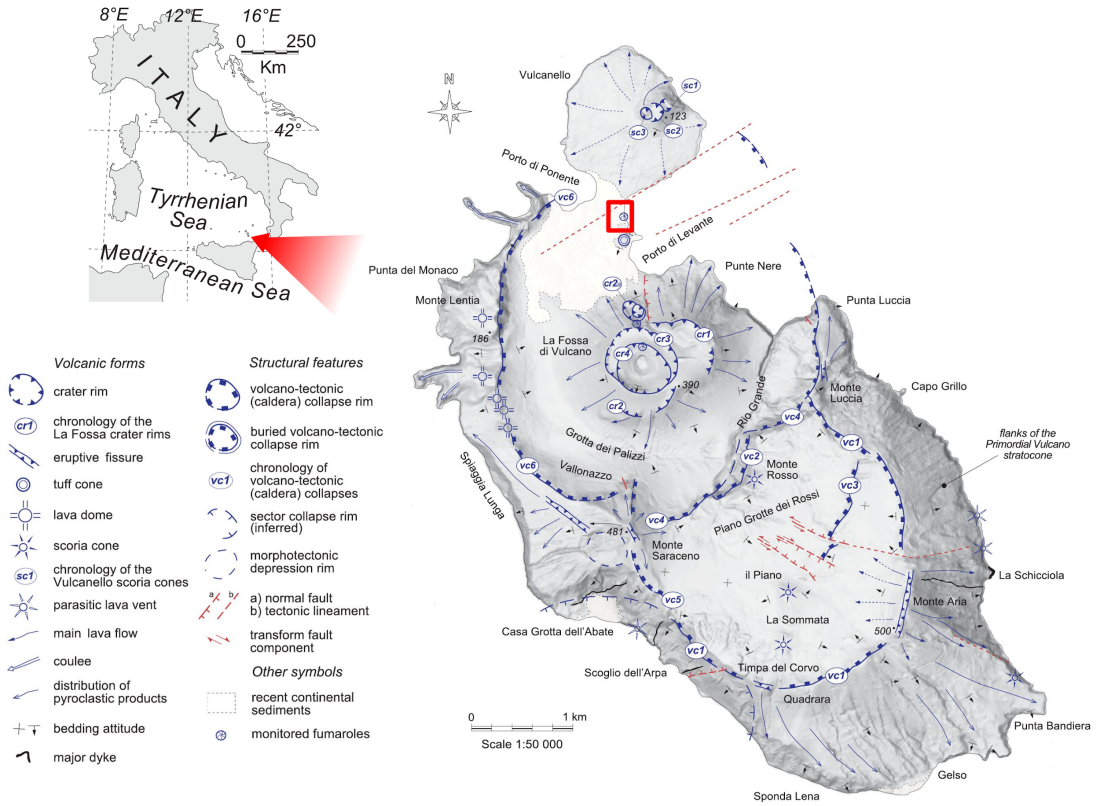

Fig. 1: Vulcano island: its location, geological features and the location of the measurement site marked as a red rectangle (De Astis et al., 2013).

The northernmost part of the island is formed by a three-stage vulcano, the Vulcanello, which is connected to the main part of the island by an isthmus, the so called 'Dead Field'. The measurement site was located at the eastern beach, right within the area of the Dead Field. The place is characterized by various active fumaroles which affect the electrical conductivity of the subsurface by migration of volcanic gases in saline water. This results in an highly conductive, corrosive regime that is coupled with resistive gas bubbling - a challenge for both SIP and TEM.

2 Vulcano Porto Beach Fumaroles

Beneath the Dead Field, a broad fault zone is located striking from SW to NE. This area provides various migration paths for volcanic gases. Rising gases pass through a thermal aquifer in approximately 200m depth and heat up. Depending on whether they mix with shallow groundwater and infiltrated sea water on their further rise or not, the resulting gas discharges can be both hot and cool. Therefore, both discharge phenomena are characterized by temperatures between 40 – 100°C, which may vary at very small spatial distances over the entire temperature range (Baubron et al., 1990; Capasso et al., 2001; Taran, 2011). They further occur both onshore and offshore (Fig. 2). Since they originate from the same deep source, the escaping gases are all composed of CO_2 and up to 0.4% H_2S. Due to the acidifying gases, waters close by the fumaroles have reduced pH values (3 - 4.5 at the investigated fumarole field).

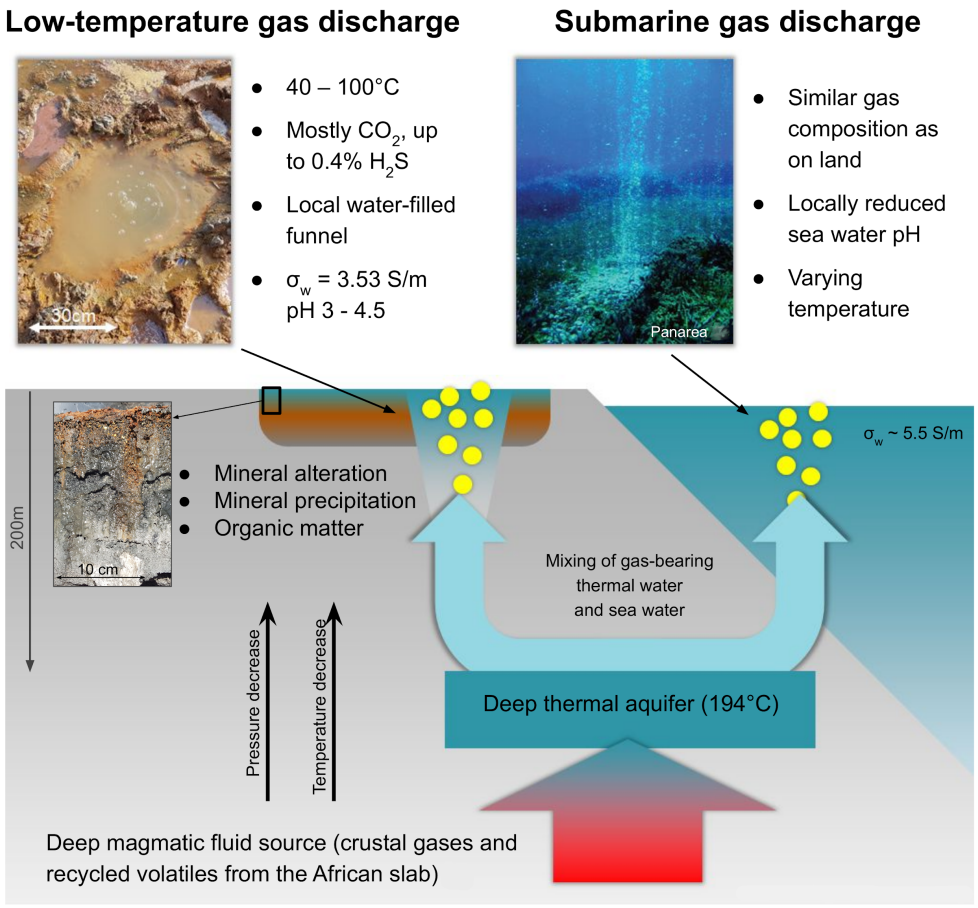

Fig. 2: Schematic classification of the current fumaroles at the Dead Field based on (Baubron et al., 1990; Capasso et al., 2001; Taran, 2011; Merkel et al., 2011). Top right figure from Merkel et al. (2011).

3 Electrical conductivity

In general, the electrical conductivity of rocks and soils σ^* has to be considered as a frequency dependent, i.e. complex quantity (Olhoeft, 1985). σ^*, which is related to complex resistivity ρ^* by the reciprocal, can be expressed in terms of real and imaginary part (σ', σ'') or as amplitude and phase shift ($|\sigma^*|$, φ).

$$\sigma^* = \frac{1}{\rho^*} = \sigma' + \sigma'' = |\sigma^*| \cdot e^{i\varphi} \tag{1}$$

The real part σ' is dominated by the electrolytic conductivity, which is commonly described by the empirical Archie's law. It depends on porosity Φ, pore water conductivity σ_w and brine saturation $S_\mathrm{w} = 1 - S_\mathrm{gas}$ (Archie, 1942). Archie's law only fully for clay-free, sedimentary rocks.
The imaginary part σ'' originates from the interface conductivity and reflects the polarization properties of mineral-water interfaces. σ'' depends on pore water conductivity, the pH, the occurrance of highly polarizable minerals θ_pol (such as e.g. some sulphides), and the internal surface area A.

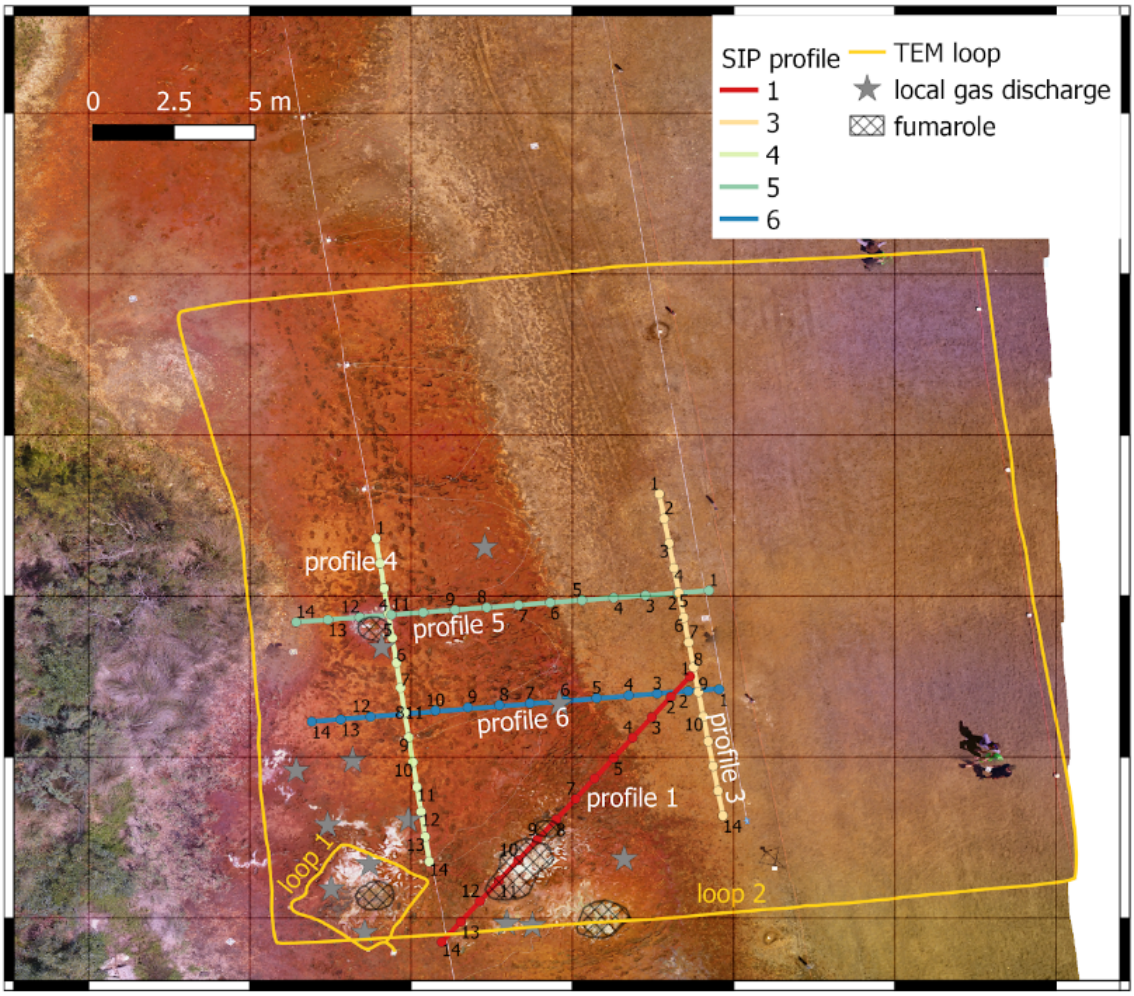

Fig. 3: Measurement site at the Dead Field beach. Yellow loops denoting the current coils of the TEM measurements, colored lines denote the SIP profiles and the points on those the respective electrode position.

The presence of fumaroles, i.e. the associated CO2-rich gas discharges, can have multiple impacts on the complex conductivity σ^*. For instance, changes in the local porosity due to fluid migration pathways or mineral precipitation and partial saturation ($S_{\text{gas}} > 0$) due to gas bubbles strongly modify the electrolytic conductivity. Variations of pore water conductivity σ_{w} due to groundwater or seawater mixing as well as reactive gas dissolution and dissociation affect both the electrolytic and interface conductivity. Gas dissolution or dissociation processes moreover cause acidification which mainly act on σ'' (Börner et al., 2015, 2017). Furthermore, variations in the internal surface area A due to mineral alteration or precipitation processes and an increase in polarizable components θ_{pol} due to the presence of either organic matter (e.g. from dead plants), altered minerals (e.g. clay minerals), or precipitated minerals (e.g. pyrite, limonite) can influence the interface conductivity.

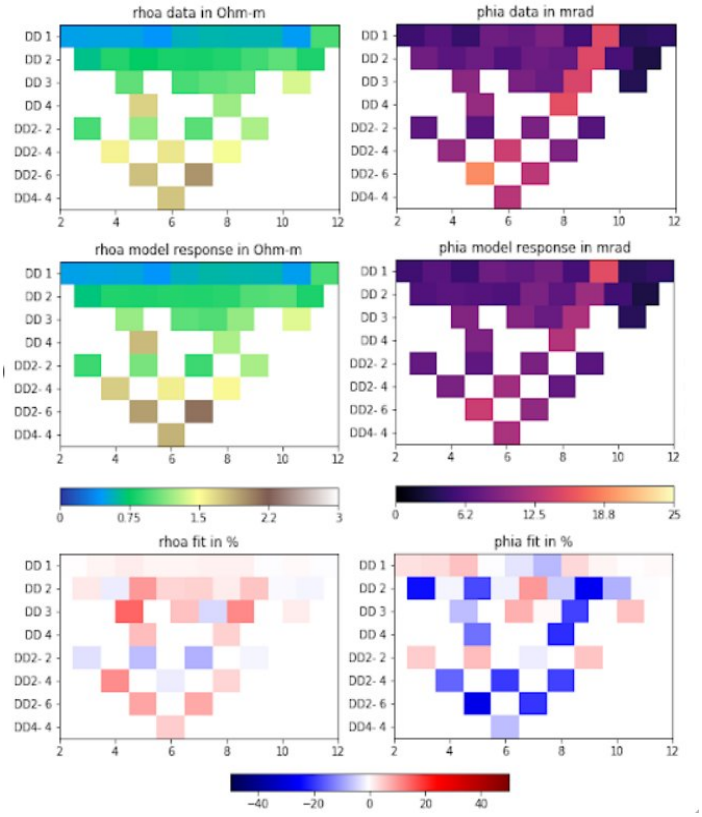

Fig. 4: Measured SIP data (top row), resulting model response (middle row) and data fit for Profile 1 at 23.4 Hz.

4 SIP measurements

To grasp the presence of the fumaroles by its polarization effects, SIP measurements on 5 profiles (see Fig. 3) were carried out, using a SIP 256D (Radic Research) instrument. The survey comprised dipole-dipole configuration measurements with a spacing of 1 m and a frequency range of 91.5 mHz to 20 kHz. Because of the special setting of the Vulcano Porto beach fumaroles it was necessary to face many experimental challenges. The measuring device was endangered by the corrosive environment (low pH) and the high surface temperatures due to insolation. The high conductivity of the upper layer and the noise (anthropogenic as well as from the gas bubbling) had a big influence on data quality and feasibility of the measurements in general.

The received data was processed with a single frequency inversion using the PyGimli framework and a two-step IP inversion approach (Oldenburg & Li, 1994; Rücker et al., 2017). The underlying algorithm is based on a Gauss-Newton (GN) approach with a CGLS solver, incorporating a data weighting based on the measured errors. Furthermore, smoothness constraints, a regularization parameter reduction at each GN step, and a line search approach for controlling the model updates were exploited. 4 a data selection on Profile 1, illustrating the challenging, highly conductive environment in the raw data already. In particular, the phase measurements turned out to be difficult due to the high conductivities. Data with errors above 20% have been discarded. The inversion result, shown in Fig. 5, considers Profile 1 and is exemplary for the whole survey. The

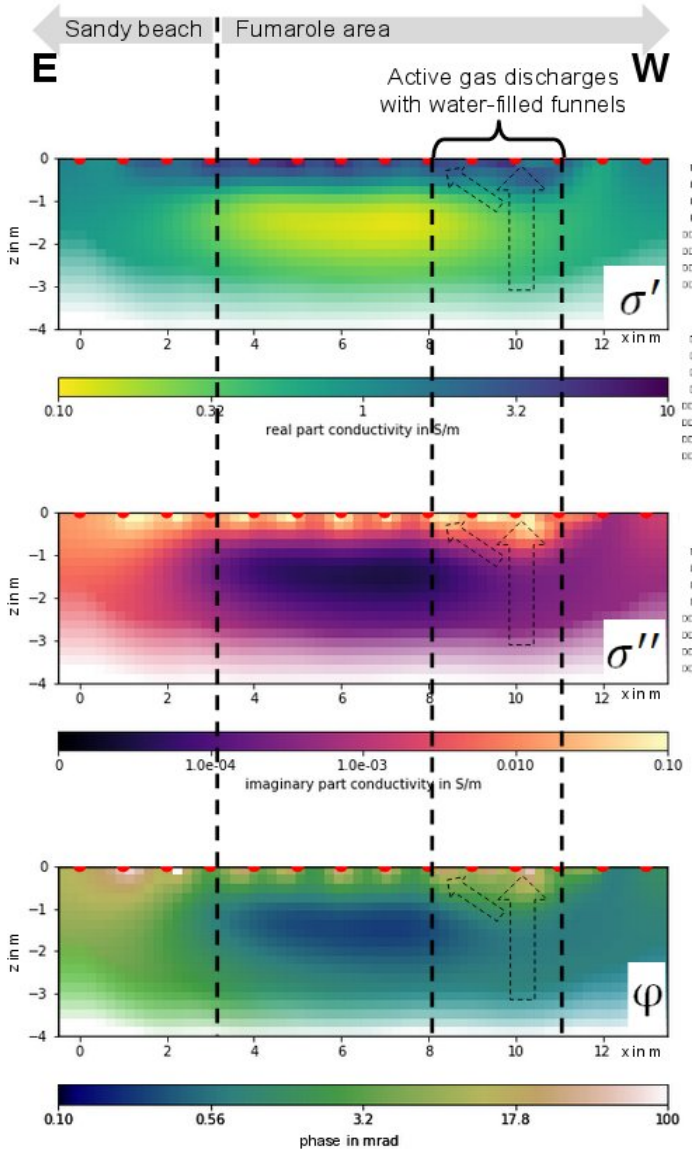

Fig. 5: Inversion results for Profile 1 at 23.4 Hz

illustrated spatial parameter distributions are obtained after 5 GN iterations (relative final objective function: 0.67%) for the apparent resistivity and 27 GN iterations (relative final objective function: 0.41%) for the imaginary part of resistivity. The phase and imaginary conductivity have been computed during post-processing.
Focusing on the profile section between 8 and 11 m, i.e. the area where the visible fumarole is located at the surface, an indication on it is given as a zone of increased real conductivity and polarization strength at depth. It is assumed that these characteristics mainly arise from the local gas discharge. The high porosity at the uppermost layers favour a high saturation with the highly conductive groundwater which lead to an increase in σ' close to the surface. Furthermore, the presence of organic matter and iron-rich precipitations lead to high amplitudes, also in the components of σ'' and φ.

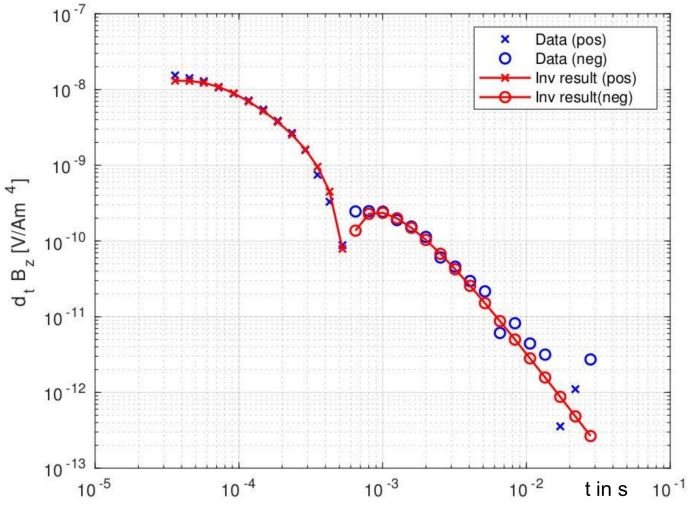

Fig. 6: Data (blue) and inversion result (red) of the separate loop measurements at a distance of r = 40 m.

5 TEM measurements

The TEM soundings were conducted using a Geonics PROTEM 47 device. Two different loop positions were set up. Loop 1 (see Fig. 3) with a side length of approx. 3 m in order to investigate the temporal effect in TEM measurements of the underlying fumarole exhibiting strong gas bubbling, and Loop 2 (see Fig. 3) with a side length of 40 m to map the 1D background conductivity structure. Two different measurement configurations were used at each site: an inloop configuration in the center of the transmitter loop and a separate loop configuration at a distance of 40 m north of the center of the transmitter loop. During the measuring process, current monitoring was applied to successfully correct temperature induced power anomalies during data processing.
Due to the abundance of meteoric and salt water as well as corrosive gases, the whole measurement had to be handled with extreme care to avoid damage to the instrumentation. Furthermore, a highly conductive regime limits the accessible depth range of TEM measurements. The TEM signal is provided by eddy currents in the underground propagating downward in time. However, in high conductivity regimes the current propagates with low velocities, it is trapped within the conductive layer. Additionally, several noise sources were present at the location. In addition to anthropogenic noise including water supply pumps, buried pipes and power cables, the fumaroles' gas bubbling contributes to an intermediate signal-to-noise-ratio.
For TEM data inversion, a stack of ten time series of the data measured in separate loop configuration using Loop 2 was chosen. They were accomplished using a square transmitter loop source of length 23 m by 23 m and a current of 3 A. The receiver was located 40 m north of the center of the transmitter loop. Taking into account a low resistivity of 1 Ωm, the penetration depth is approximately 30 m. As a starting model for inversion a 10 layered homogeneous half-space of 10 Ωm was defined. The inversion based on a 1D damped Gauss-Newton approach terminated after 28 iterations. The result is shown in Fig. 6. The inversion result fits the data clearly visible. The corresponding final relative objective function has a value of 2.55%.

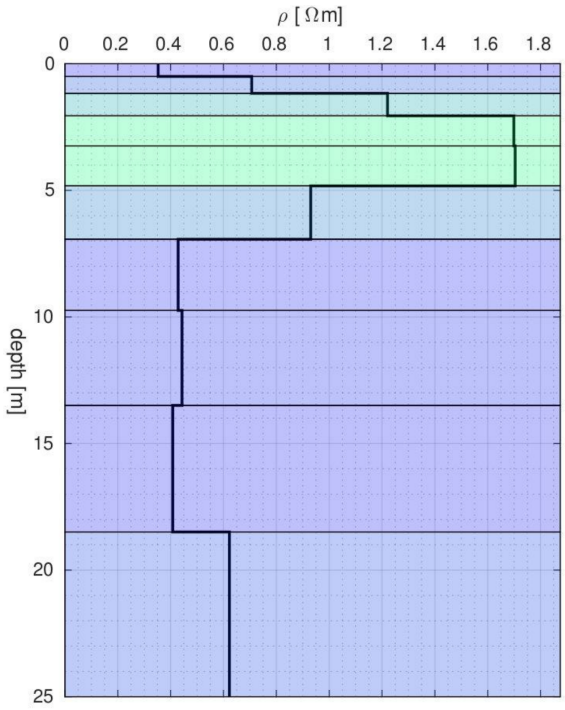

Fig. 7: Resistivity distribution as suggested by the inversion result.

As can be seen in the final resistivity model in Fig. 7, the subsurface at the location consists of three main layers: The uppermost layer seems to be a highly conductive 0.3 Ωm layer of 0.5 m thickness followed by a more resistive 2-3 m layer of 1.7 Ωm thickness. The underlying half-space appears to have a resistivity of 0.6 Ωm. Overall, this section can be regarded as a highly conductive regime.

6 Discussion and conclusion

The resulting conductivity models from both methods (Figs 5 and 7) show very consistent results despite their different length scales and sensitivities. Both methods reconstruct a conductivity of approximately 3 S/m close to the surface. Given the muddy, highly-porous ground and the surface water conductivity of 3.53 S/m (cf. Fig. 2), this can be considered realistic. Furthermore, both methods show a zone of slightly lower conductivity in 1 to 5 m depth. The TEM, which has the greater penetration depth, reconstructs a conductivity increase below 5 m. The overall very high conductivities and the therefore low penetration depth do not allow for resolving the bed rock. The slight conductivity variations below 1 m depth could e.g. be caused by the mixing of sea and ground water.
The present article reports on a successful joint application of SIP and TEM measurements in a noisy and highly corrosive environment of a fumarole field. Preliminary inversion results of both EM methods show a high consistency in the background conductivity. Furthermore, these results allow for first implications that small scale CO2 discharges in a highly conductive environment can be mapped with electromagnetic methods.
Future investigations will first include a comparison with SIP lab measurements of local soil. Furthermore, 3D inversion of the entire SIP data set and 1D inversion of all TEM

components (x, y, z) as well as an attempt of a SIP-TEM joint inversion are considered. In case of validation of the first evidence of detectability, investigation of gas discharges at different life stages by a monitoring are planned.

7 Acknowledgements

This work is funded by, the Europlanet program of the European Union, the German Research Foundation (DFG, grant numbers SP 356/14-2 and RE 1705/14-2), the Ministry of Education and Research (grant 03G0843), and the European Union - European Social Fund (ESF) (GEOSax project, application number 100310486). The authors would also like to thank the organizing team of Jacobs University (Bremen) and DLR (Berlin) for realizing the Vulcano Summer School 2019.

References

Archie, G. E. (1942). The electrical resistivity log as an aid in determining some reservoir characteristics. *Transactions of the American Institute of Mining, Metallurgical and Petroleum Engineers*, *146*(146), 54–62.

Baubron, J., Allard, P., & Toutain, J. (1990). Diffusive volcanic emissions of carbon dioxide from Vulcano Island, Italy. *Letters to Nature*, *344*, 51 - 53.

Börner, J. H., Bär, M., & Spitzer, K. (2015). Electromagnetic methods for exploration and monitoring of enhanced geothermal systems – a virtual experiment. *Geothermics*, *55*(0), 78 – 87.

Börner, J. H., Herdegen, V., Repke, J.-U., & Spitzer, K. (2017). Spectral induced polarization of the three-phase system CO_2–brine–sand under reservoir conditions. *Geophysical Journal International*, *208*(1), 289 – 305.

Capasso, G., Alessandro, W. D., Favara, R., Inguaggiato, S., & Parello, F. (2001). Interaction between the deep fluids and the shallow groundwaters on Vulcano Island (Italy). *Journal of Volcanology and Geothermal Research*, *108*, 187 - 198.

De Astis, G., Lucchi, F., Dellino, P., La Volpe, L., Tranne, C., Frezzotti, M., et al. (2013). Geology, volcanic history and petrology of vulcano (central aeolian archipelago). *Geological Society, London, Memoirs*, *37*(1), 281–349.

Merkel, B., Kummer, N. S., Planer-Friedrich, B., Pohl, T., & Schipek, M. (2011). Development of a gas sampling technique for determining trace elements in submarine volcanic exhalations. *Procedia Earth and Planetary Science*, *4*, 50 - 56.

Oldenburg, D. W., & Li, Y. (1994). Inversion of induced polarization data. *Geophysics*, *59*(9), 1327–1341.

Olhoeft, G. R. (1985). Low-frequency electrical properties. *Geophysics*, *50*, 2492–2503.

Rücker, C., Günther, T., & Wagner, F. M. (2017). pygimli: An open-source library for modelling and inversion in geophysics. *Computers & Geosciences*, *109*, 106–123.

Taran, Y. A. (2011). N2, Ar, and He as a tool for discriminating sources of volcanic fluids with application to Vulcano, Italy. *Bulletin of Vulcanology*, *73*, 395 - 408.

Unnithan, V., Thomsen, L., Sohl, F., Baqué, M., Gwinner, K., Haber, J., et al. (2019). *Vulcano summer school 2019.*